Species	Sterilization protocol	Stratification	Etiolation period	Container type/medium volume	PTFE raft mesh type	Seeds per raft	–Fe condition initial $FeSO_4$ content (µM)	Medium exchange (d)	Harvest (d)
Arabidopsis thaliana	**1:** 20% bleach + 0.1% Tween 20 for 5 min, 3 water washes	**1:** 4°C for 2 days	72 h	**1:** 6-well plate, 3 mL per well	**1:** 0.025" x 0.005"	16	10	8	12
Eutrema salsugineum	**1**	**2:** 4°C for 20 days	72 h	**1**	**1**	16	10	10	18
Brassica rapa	**1**	**1**	-	**2**: Magenta box, 36 mL per box	**3:** 0.080" x 0.025"	9	0	16	28
Nicotiana benthamiana	**1**	**1**	-	**1**	**1**	16	0	-	16
Leucanthemum vulgare	**1**	**1**	-	**1**	**2:** 0.045" x 0.025"	9	0	-	16
Papaver somniferum	**1**	**1**	-	**1**	**2**	9	0	-	16
Medicago sativa	**2:** Concentrated H_2SO_4 for 12 min, 8 water washes, then 100% bleach for 30 min, 4 water washes	**1**	-	**2**	**3**	9	0	-	16

Supplementary Table 1 | Hydroponic growth conditions for tested plant species.

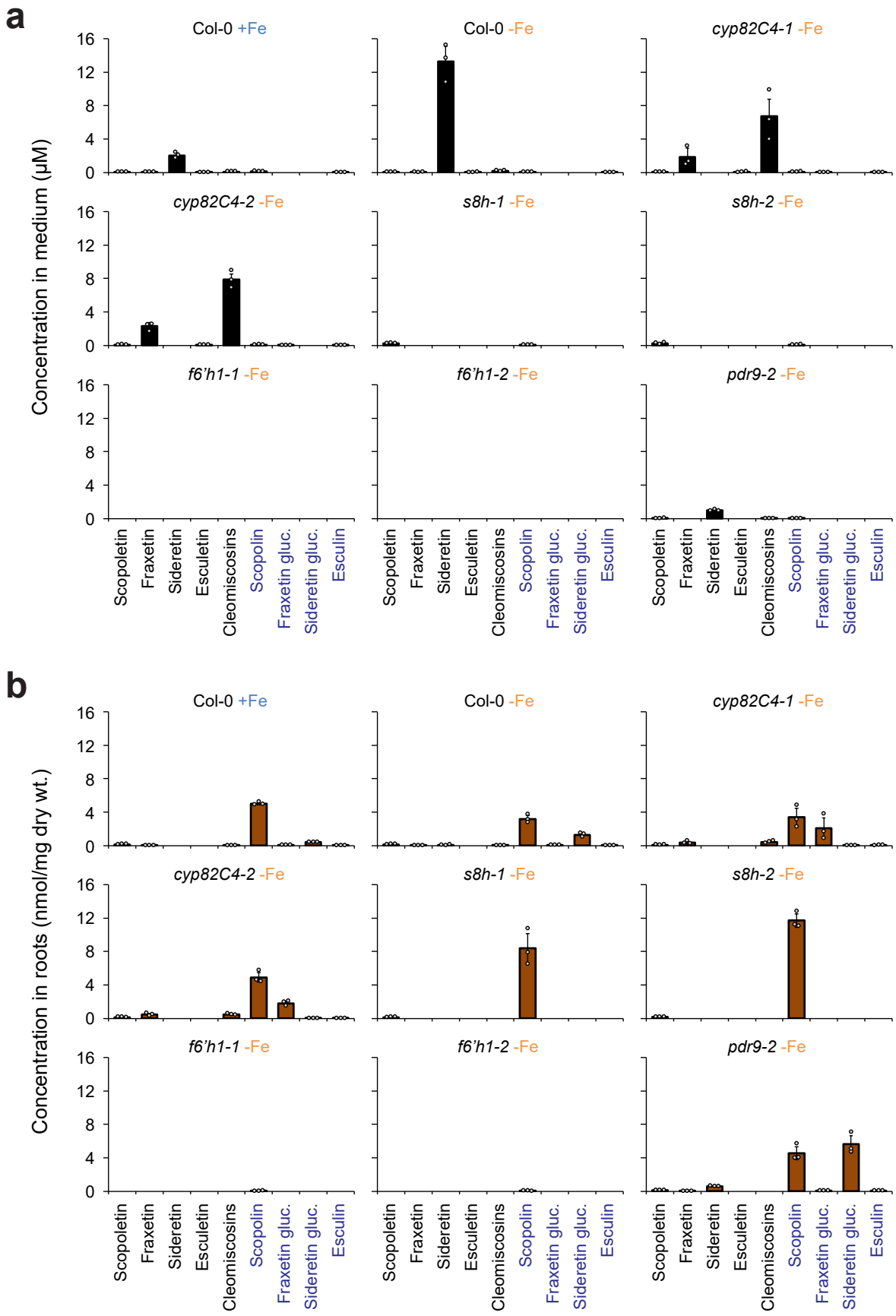

Supplementary Figure 1 (Legend on following page)

Supplementary Figure 1 | Levels of oxidized coumarins and their glucosides produced by sideretin pathway mutants. (a, b) Compound levels in spent medium (a) and roots (b) of indicated lines after 12 d of hydroponic growth at pH = 5.7. Data bars shown are mean ± s.d. for three biological replicates. Compounds for which no data points are shown were not detected. Levels of fraxetin glucosides and sideretin glucosides are approximate: for fraxetin glucosides, the ionizability of all isomers was assumed to be the same as for the commercially available fraxetin-8-*O*-glucoside (fraxin), while for sideretin glucosides, where no standard is available, the ionizability was estimated by comparing glucosidase-untreated and glucosidase-treated samples in a reconstitution experiment in *N. benthamiana*.

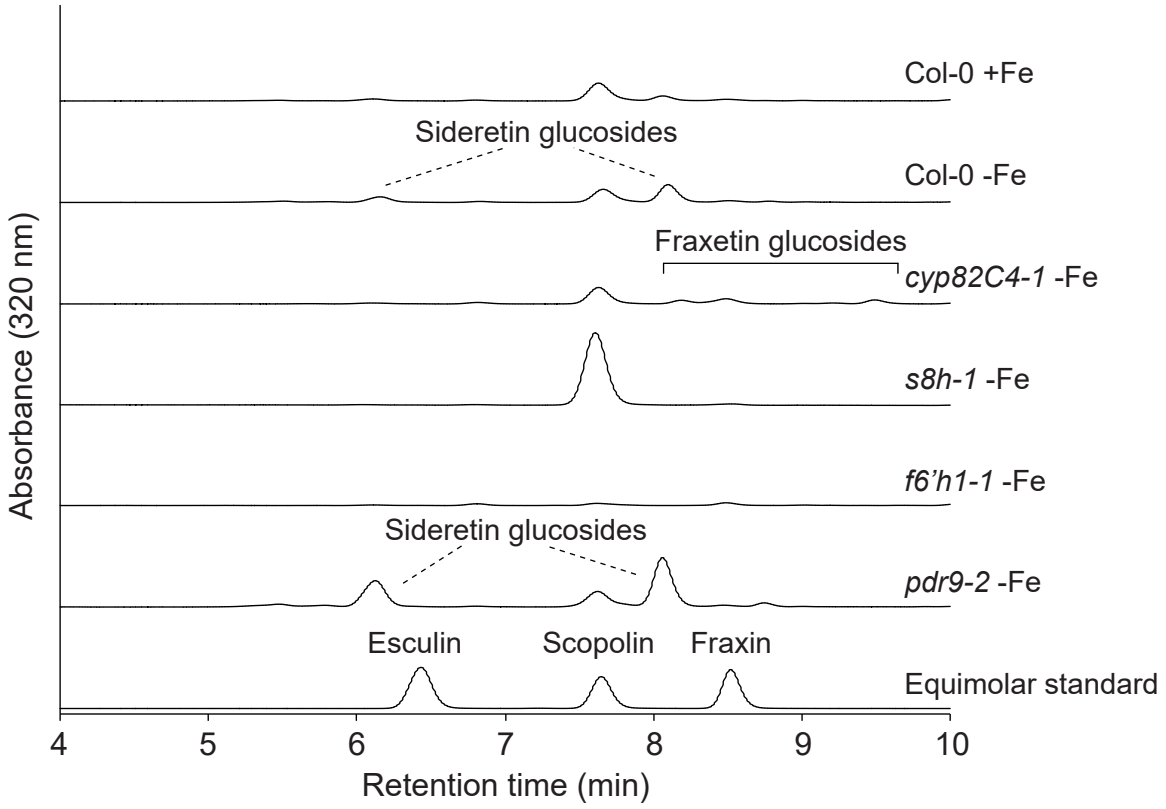

Supplementary Figure 2 | UV-Vis absorbance traces of root extracts for wild-type and mutant plants. Traces are representative of three biological replicates.

a

Rank	Locus	Annotation	Rel. expression (hr) 0 3 6 12 24 48 72	Slope
1	At1g77120	ADH1 (ALCOHOL DEHYDROGENASE 1)		0.084
2	**At3g12900**	**Oxidoreductase, 2OG-Fe(II) oxygenase family protein**		**0.083**
3	At4g33070	Pyruvate decarboxylase, putative		0.074
4	At4g02330	Pectinesterase family protein		0.072
8	At1g56430	Nicotianamine synthase, putative		0.061
13	At1g05680	UDP-glucoronosyl/UDP-glucosyl transferase family protein		0.057
18	At3g43190	SUS4; UDP-glycosyltransferase/sucrose synthase/transferase		0.053
19	**At4g31940**	**CYP82C4; cytochrome P450**		**0.053**
20	At5g36890	Glycosyl hydrolase family 1 protein		0.052
25	At2g23170	GH3.3; indole-3-acetic acid amido synthetase		0.050
27	At4g36430	Peroxidase, putative		0.050
29	At2g30750	CYP71A12; cytochrome P450		0.048
31	At1g17180	ATGSTU25; glutathione S-transferase		0.048
35	At2g43570	Chitinase, putative		0.047
37	At5g42830	Transferase family protein		0.046
42	At5g39580	Peroxidase, putative		0.045
44	At2g03760	ST (steroid sulfotransferase)		0.044
50	At5g57220	CYP81F2; cytochrome P450		0.043
52	At4g17260	L-lactate dehydrogenase, putative		0.043
53	At3g50740	UGT72E1; UDP-glucosyl transferase		0.043
55	At5g04950	Nicotianamine synthase, putative		0.043
56	**At3g13610**	**Oxidoreductase, 2OG-Fe(II) oxygenase family protein (F6'H1)**		**0.043**
57	At5g19550	ASP2 (ASPARTATE AMINOTRANSFERASE 2)		0.043
61	At1g43800	Acyl-(acyl-carrier-protein) desaturase, putative		0.042
65	At3g21240	4CL2 (4-coumarate:CoA ligase 2)		0.042
256	**At3g53480**	**ATPDR9/PDR9 (PLEIOTROPIC DRUG RESISTANCE 9)**		**0.027**
455	**At4g19690**	**IRT1 (IRON-REGULATED TRANSPORTER 1)**		**0.022**
3121	**At4g30190**	**AHA2 (Arabidopsis H(+)-ATPase 2)**		**0.011**

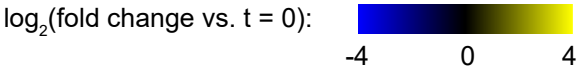

b

Rank	Locus	Annotation	Relative expression (abiotic stress type) Cold Drought Genotox. Heat Osmotic Oxid. Salt UV-B Wound.	$r_{CYP82C4}$
0	**At4g31940**	**CYP82C4**		**1.000**
1	**At4g19690**	**IRT1**		**0.890**
9	**At3g12900**	**2-ODD enzyme**		**0.619**
22	At5g58784	Dedol.-PP synthase		0.498
23	At5g03760	β-Mannan synthase		0.497
29	At1g19900	Glyoxal-oxidase related		0.482
31	At3g50740	UGT72E1		0.479
35	At3g07330	Cellulose synthase		0.476
37	At4g15360	CYP705A1		0.474

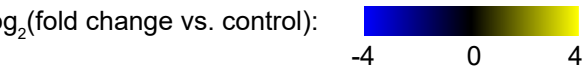

Supplementary Figure 3 | Transcriptomics analysis in *A. thaliana* for identification of candidate sideretin biosynthetic enzymes. (a) Relative induction of gene expression in roots under iron deficiency. Genes are sorted by slope of log-normalized fold change vs. time. Data from Dinneny et al.[43] (b) Gene expression under various stress conditions in roots. Genes are sorted by correlation (Pearson's *r*) with *CYP82C4*. Data from the AtGenExpress series.[42] In both panels, only enzyme-encoding genes are shown.

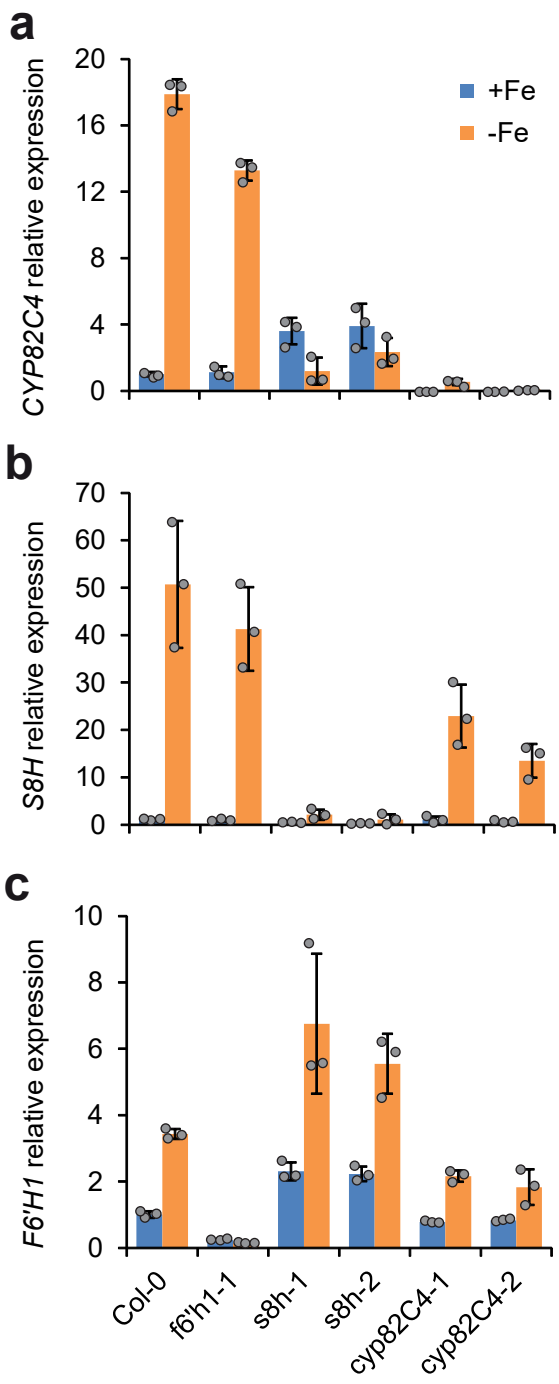

Supplementary Figure 4 | Iron-dependent regulation of *F6'H1*, *S8H*, and *CYP82C4* expression in roots. (a-c) Relative expression levels analyzed by qPCR of *CYP82C4* (a), *S8H* (At3g12900) (b) and *F6'H1* (c) in roots of wild-type (Col-0) or indicated mutants after 6 days of treatment. Seedlings were pre-cultured for 7 days on half-strength MS medium (75 µM Fe-EDTA) and transferred to fresh half-strength MS medium containing 75 µM Fe-EDTA (+Fe) or no added Fe plus 15 µM of the Fe chelator ferrozine (-Fe). Expression of the housekeeping gene *UBQ2* served as reference in all assays. Data represent the mean ± s.d. of three independent root pools (collected from 15 plants).

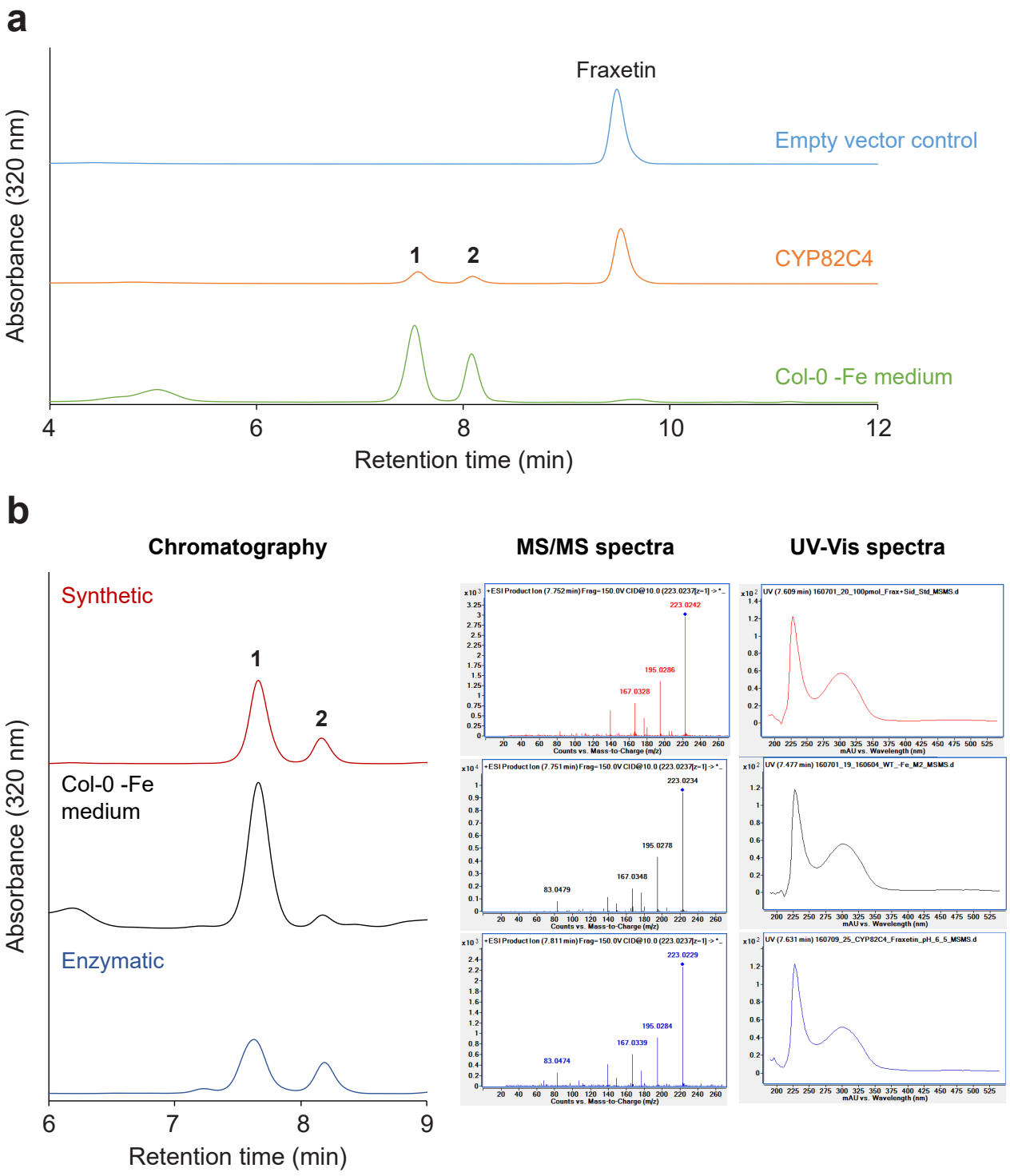

Supplementary Figure 5 | Incubation of fraxetin with CYP82C4 yields sideretin *in vitro*. (a) UV-Vis absorbance traces of enzymatic reactions with fraxetin show that the major peaks seen in wild-type exudates (**1**, **2**) arise via hydroxylation of fraxetin by CYP82C4. The experiment was repeated two times with similar results. (b) Retention time comparisons, MS/MS fragmentation patterns, and UV-Vis absorbance profiles establish the identity of sideretin from various sources. MS/MS (10 V collision energy) and UV-Vis profiles are for the oxidized species (**1**).

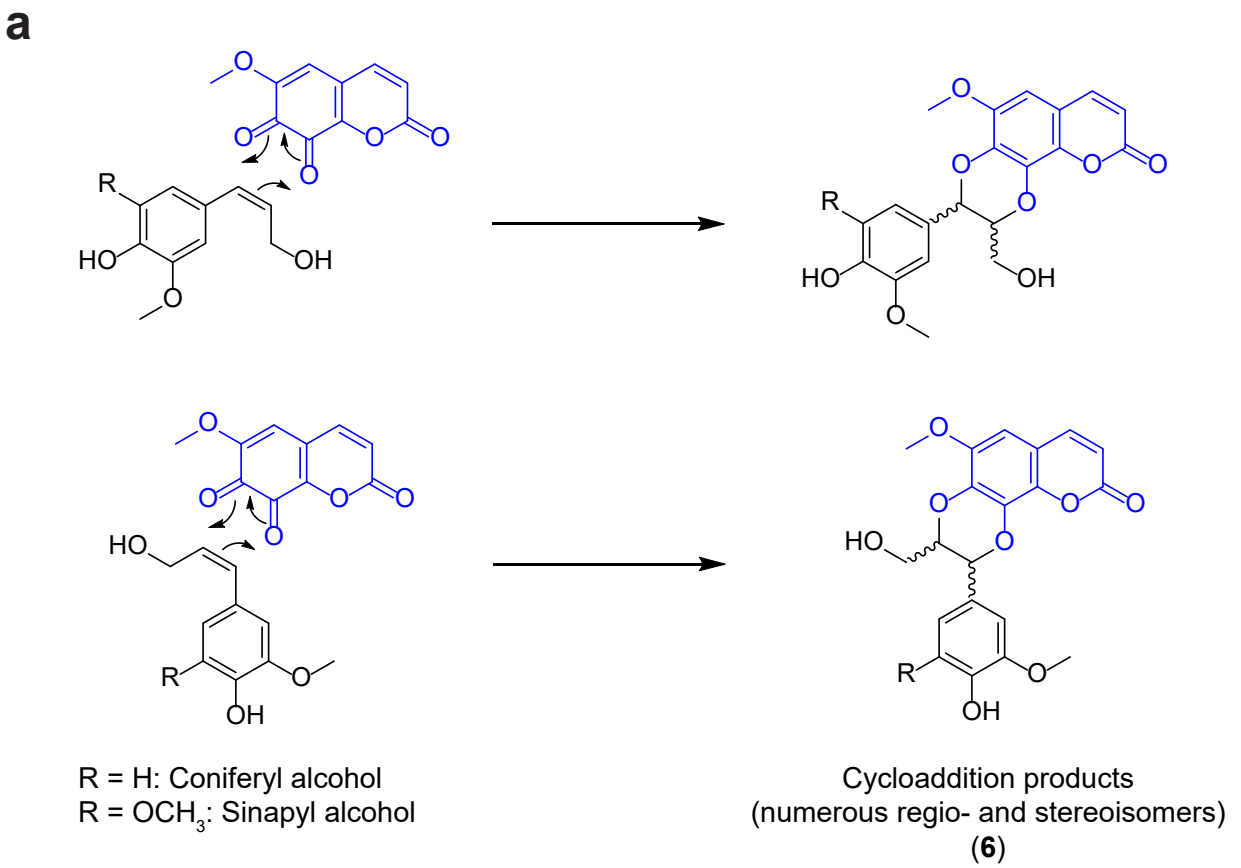

Supplementary Figure 6 | Oxidized fraxetin reacts with monolignols to generate cleomiscosins. (a) Presumed [4+2] cycloaddition reactions of oxidized fraxetin with alkene-containing monolignols. (b, c) Extracted ion chromatograms comparing retention times of compounds observed in *cyp82C4-1* spent medium and products of the oxidative coupling of coniferyl alcohol (b) (Extracted m/z $[M+H]^+$ = 387.1074; $C_{20}H_{18}O_8$) and sinapyl alcohol (c) (Extracted m/z $[M+H]^+$ = 417.1180; $C_{21}H_{20}O_9$). Note that non-specific addition would give rise to four separable isomer peaks (that is, four pairs of enantiomers) for each synthesis, as observed in the EIC traces.

a

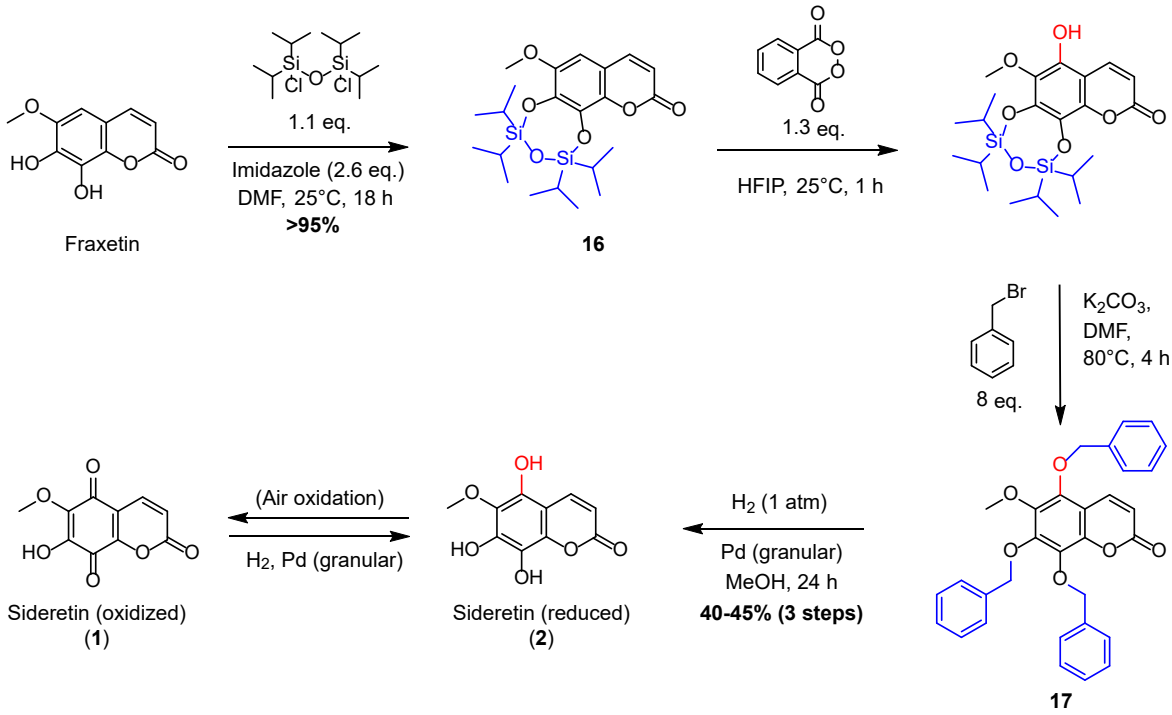

b

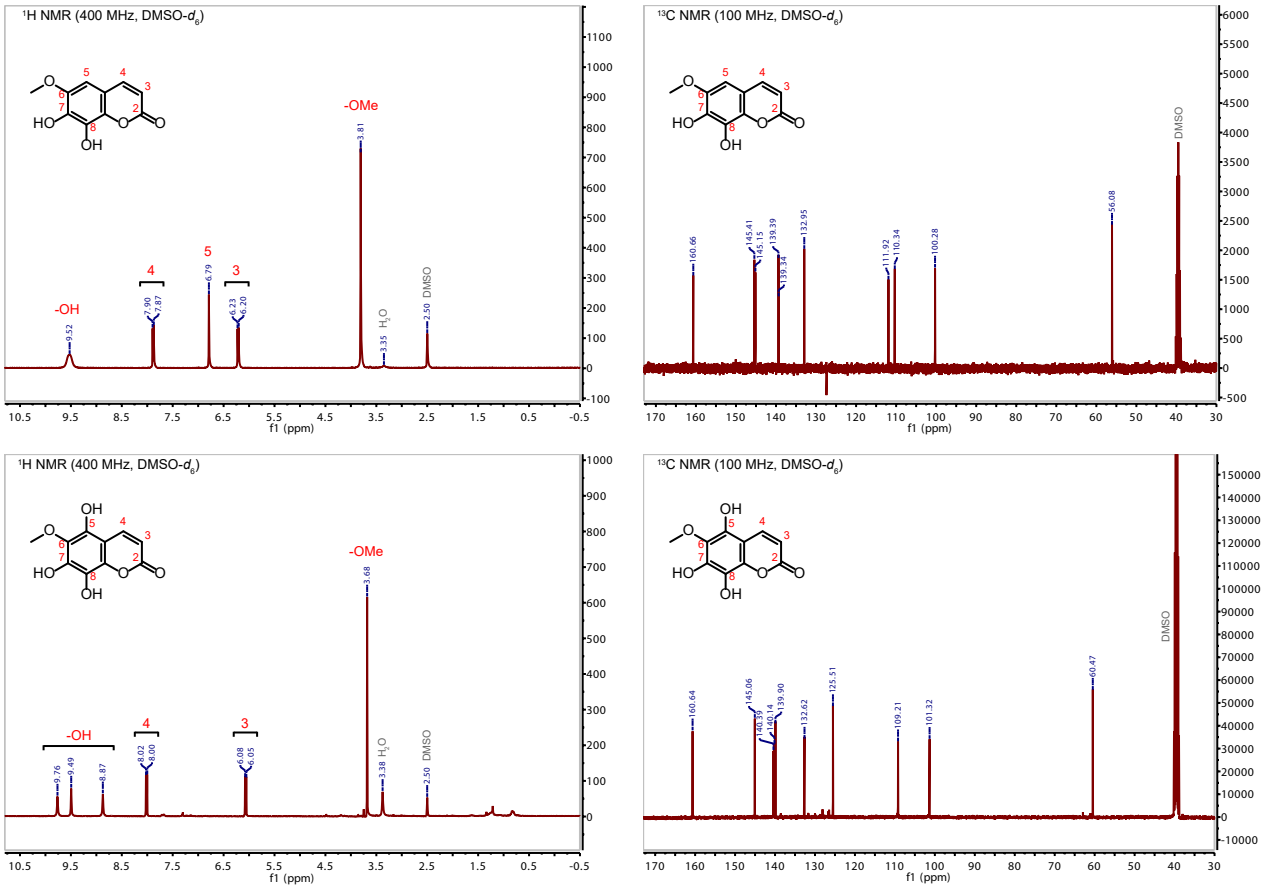

Supplementary Figure 7 (Legend on following page)

Supplementary Figure 7 | Synthesis of sideretin from fraxetin. (a) Overall synthetic scheme for sideretin via phthaloyl peroxide hydroxylation of fraxetin. (b) Comparison of ^{1}H and ^{13}C NMR spectra for fraxetin standard and synthetic sideretin. Loss of the unique fraxetin aromatic resonance ($\delta = 6.79$) in the sideretin ^{1}H spectrum demonstrates that sideretin is hydroxylated at carbon 5 (standard coumarin carbon atom numbering shown).

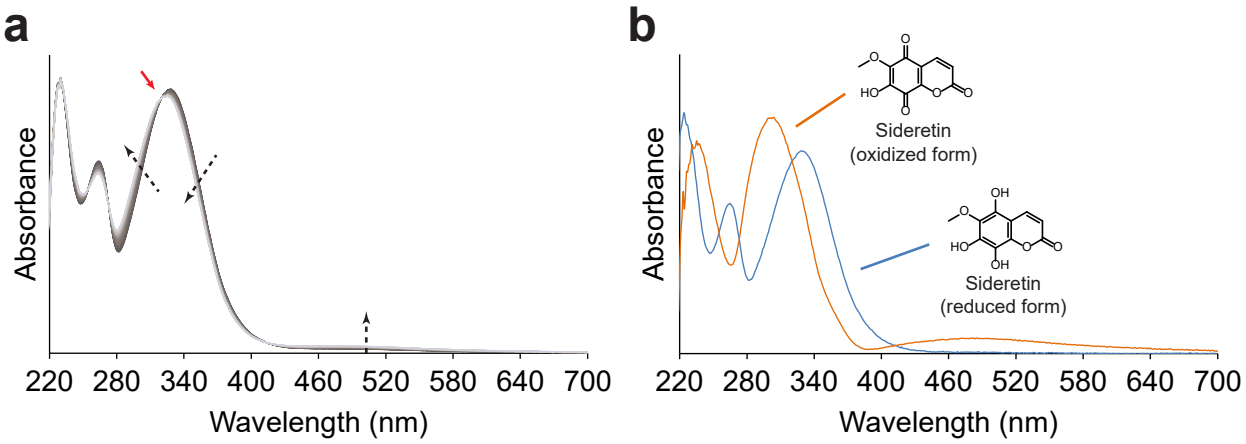

Supplementary Figure 8 | UV absorbance properties of sideretin. (a) A scanning kinetics experiment shows the progress of sideretin oxidation in air. Black arrows indicate change in absorbance with time; the red arrow indicates an isosbestic point at 320 nm. (b) UV absorbance spectra for the quinone and catechol forms of sideretin. The catechol spectrum was obtained for pure compound under anoxic conditions, while the quinone spectrum was found by deconvolution from the scanning kinetics data.

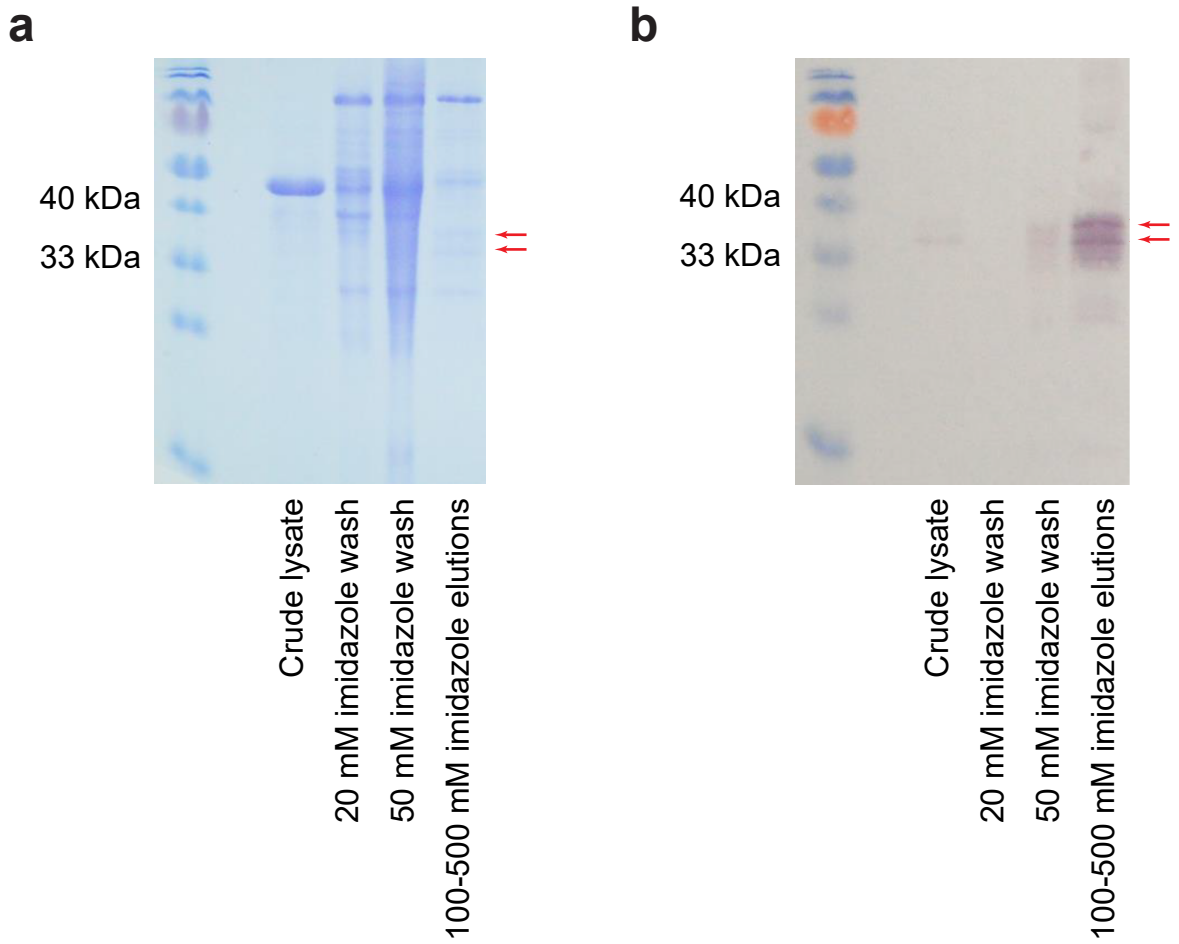

Supplementary Figure 9 | Partial degradation of *A. thaliana* S8H protein heterologously expressed in *N. benthamiana* leaves. (a, b) Coomassie-stained protein gel (a) and anti-6xHis Western blot (b) of S8H protein nickel affinity chromatography purification fractions. The predicted molecular weight of the full-length product is 41 kDa.

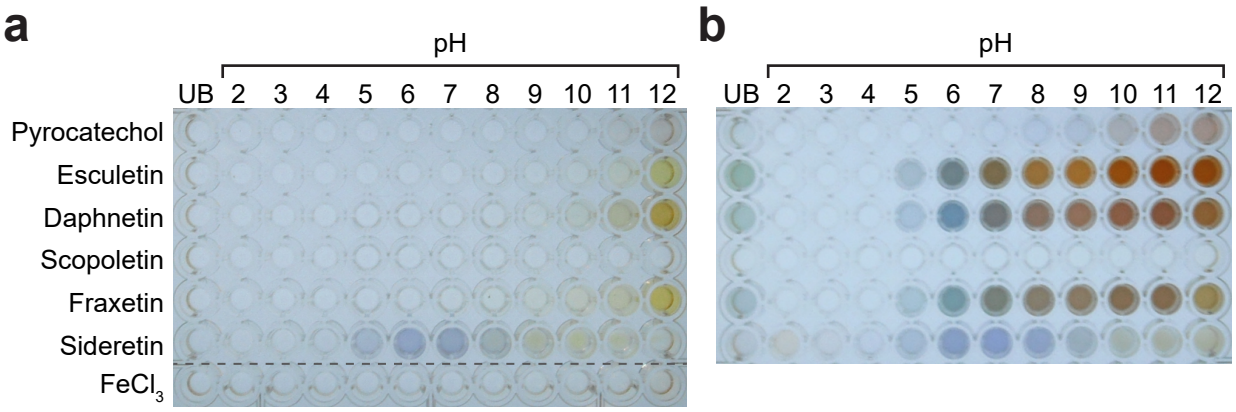

Supplementary Figure 10 | Formation of catecholic coumarin-Fe(III) complexes. (a, b) Appearance of 750 µM compound standards (250 µM for $FeCl_3$) in aqueous solution buffered with Britton-Robinson buffer at the indicated pH (a), or 5 min after addition of 250 µM $FeCl_3$ (b). Note that scopoletin, which lacks a catechol moiety, does not form a colored complex with Fe(III) at any pH; furthermore, sideretin initially forms colored complexes of comparable intensity to the other catecholic coumarins, but the color rapidly fades, suggesting that sideretin- Fe(III) complexes are unstable. UB: unbuffered.

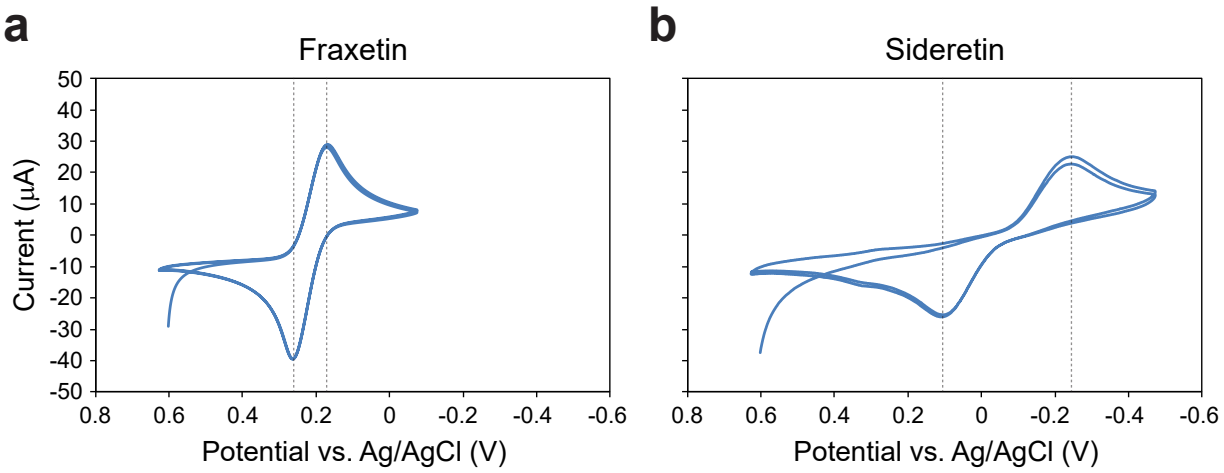

Supplementary Figure 11 | Cyclic voltammetry of fraxetin and sideretin. (a, b) Voltammetry traces for fraxetin (a) and sideretin (b) were obtained in aqueous phosphate buffer at pH 6.5. The average of the two potentials at maximal current (indicated by dashed lines) is, after correction (see Materials and Methods), a good estimate of the standard redox potential. The standard redox potentials (vs. SHE) calculated in this manner are +0.803 V for fraxetin and +0.503 V for sideretin. The experiments were repeated two times with similar results.

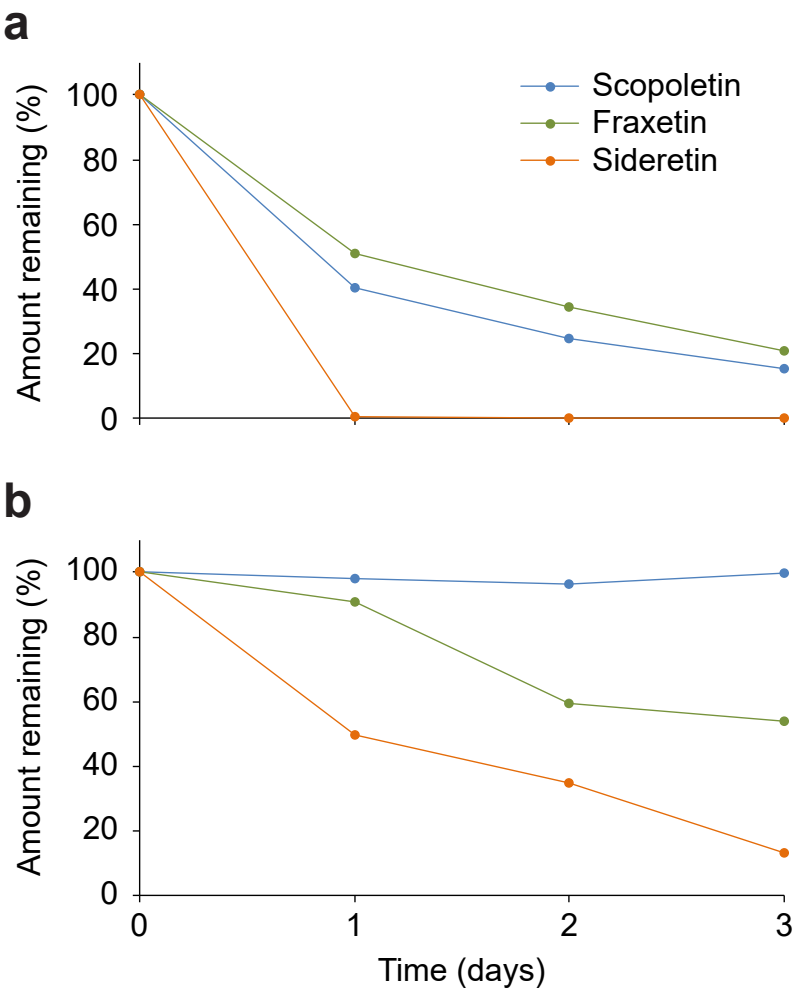

Supplementary Figure 12 | Photosensitivity of coumarins in hydroponic medium. (a, b) Coumarin degradation over time in MS medium, either under exposure to standard light conditions (16 h day cycle) in a growth chamber (a) or no light exposure (b). The experiment was repeated twice with similar results.

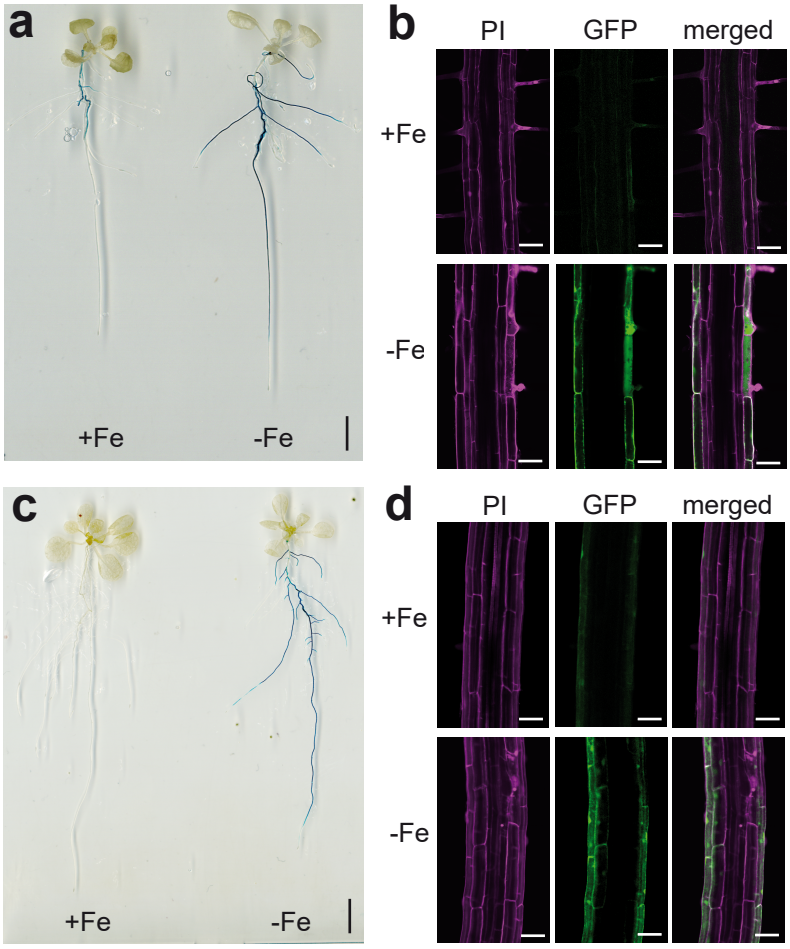

Supplementary Figure 13 | Tissue- and cell-type specific localization of *S8H* and *CYP82C4* expression. (a, b) *proS8H*-dependent GUS activity (a) and GFP expression (b) in Fe-sufficient or Fe-deficient plants. (c, d) *proCYP82C4*-dependent GUS activity (c) and GFP expression (d) in Fe-sufficient or -deficient plants. Plants were precultured in half-strength MS medium (75 µM Fe-EDTA) medium for 7 days and then transferred to half-strength MS medium with 75 µM Fe-EDTA (+Fe) or no added Fe plus 15 µM of ferrozine, a strong Fe chelator (-Fe). All plates were buffered at pH = 5.5 with 2.5 mM MES. In b and d, eight images were taken per treatment for each reporter line and representative root sections from one representative transgenic line (six independent lines per construct) are shown. Scale bars, 0.5 cm (a, c) and 50 µm (b, d). Pink fluorescence derives from propidium iodide (PI) staining of cell walls.

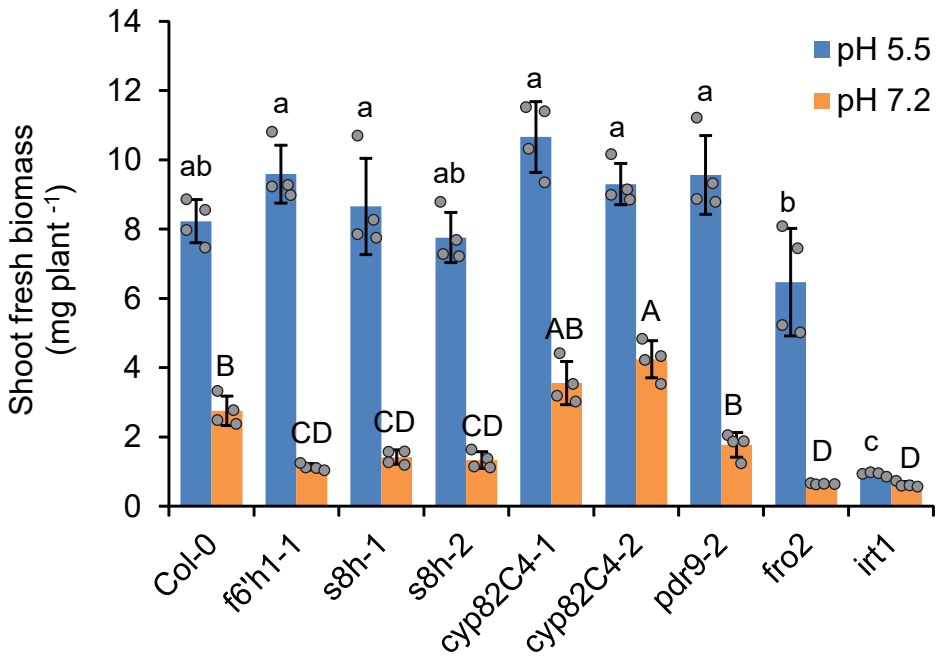

Supplementary Figure 14 | Biomass of *s8h*, *cyp82C4* and other mutants grown in soil under conditions of low Fe availability. Growth conditions as in Fig. 3a-c. Data represent mean ± s.d. of four independent replicates containing five shoots each. Different letters at pH 5.5 or pH 7.2 indicate significant differences according to one-way ANOVA with *post hoc* Tukey's test ($p < 0.05$). The experiment was repeated two times with similar results.

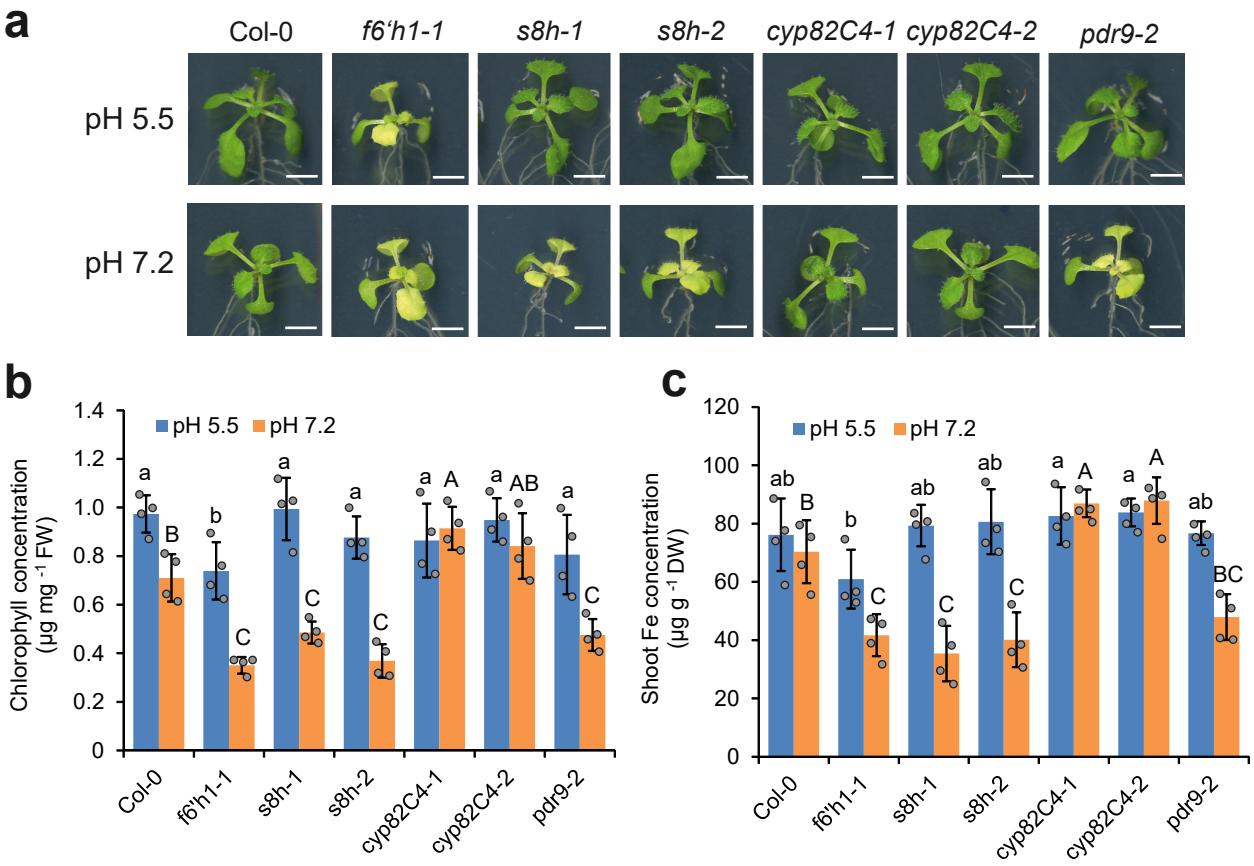

Supplementary Figure 15 | Phenotypic characterization of sideretin pathway mutants on agar. (a-c) Appearance of shoots (a), leaf chlorophyll concentration (b) and shoot Fe concentration (c) of wild-type (Col-0) and various mutant plants grown for 6 days on low Fe availability at the indicated pH. Results shown represent the mean ± s.d. of four independent replicates containing five shoots each. Different letters at pH 5.5 or pH 7.2 indicate significant differences according to one-way ANOVA with *post hoc* Tukey's test ($p < 0.05$). The experiment was repeated two times with similar results. Scale bars, 0.5 cm (a).

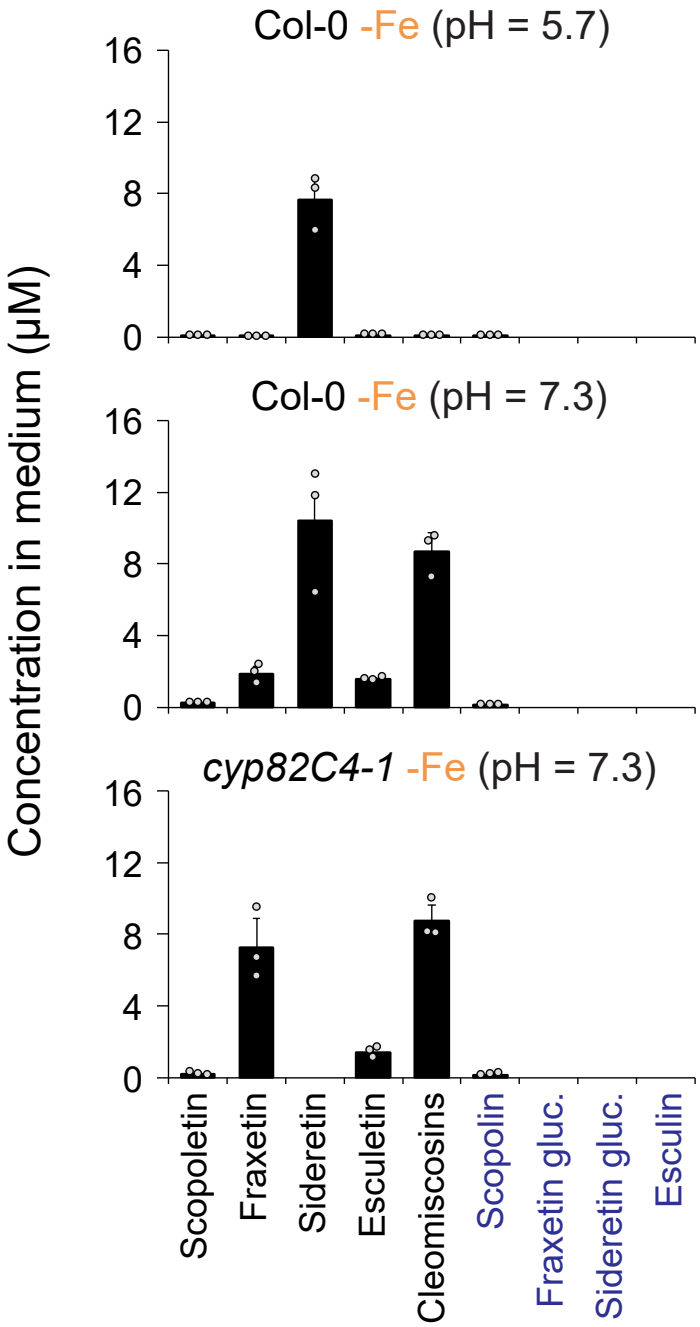

Supplementary Figure 16 | Comparison of root-exuded coumarin levels at pH 5.7 and pH 7.3. Compound levels in spent medium after 12 d of growth at the indicated pH. Data bars shown are mean ± s.d. for three biological replicates. Compounds for which no data points are shown were not detected. Levels of compounds for which exact standards are not available were determined as described in Supplementary Fig. 1.

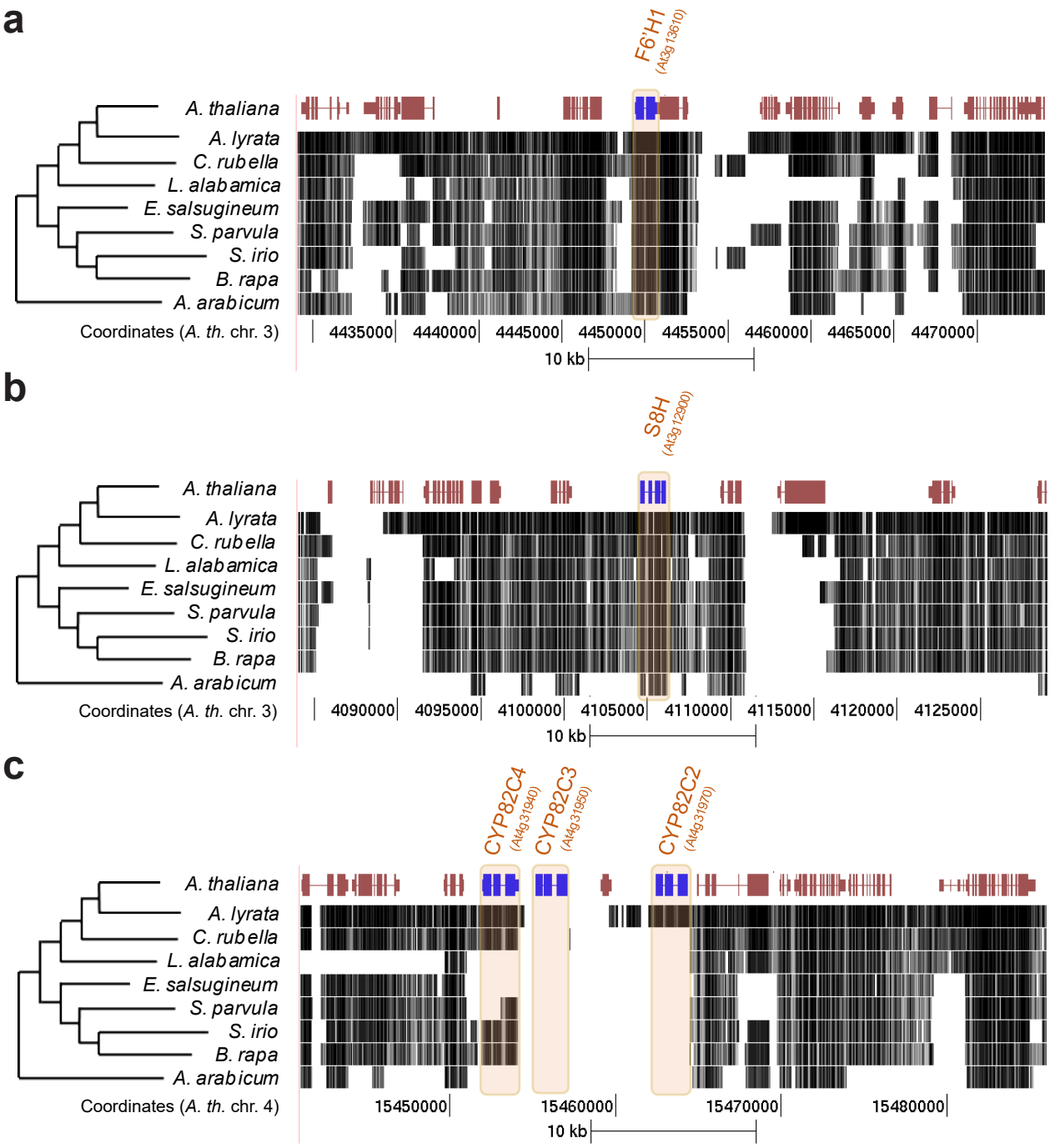

Supplementary Figure 17 | Comparative genomics for sideretin pathway genes in the Brassicaceae family. (a-c) Multiple genome alignments against *A. thaliana* sideretin pathway enzyme genes for a set of 8 sequenced plants. For *A. thaliana*, gene models from the TAIR9 release are shown. Figures were generated using the USCS Genome Browser. The *F6'H1* (a) and *S8H* (b) genes appear to be well conserved among all species in this alignment, whereas the CYP82C locus (c) shows a complex evolutionary history, marked by independent chromosomal deletions in various lineages, as well as tandem duplication and neofunctionalization in *Arabidopsis* species. Notably, *L. alabamica*, *E. salsugineum*, *S. parvula*, and *A. arabicum* all lack a complete *CYP82C4* gene.

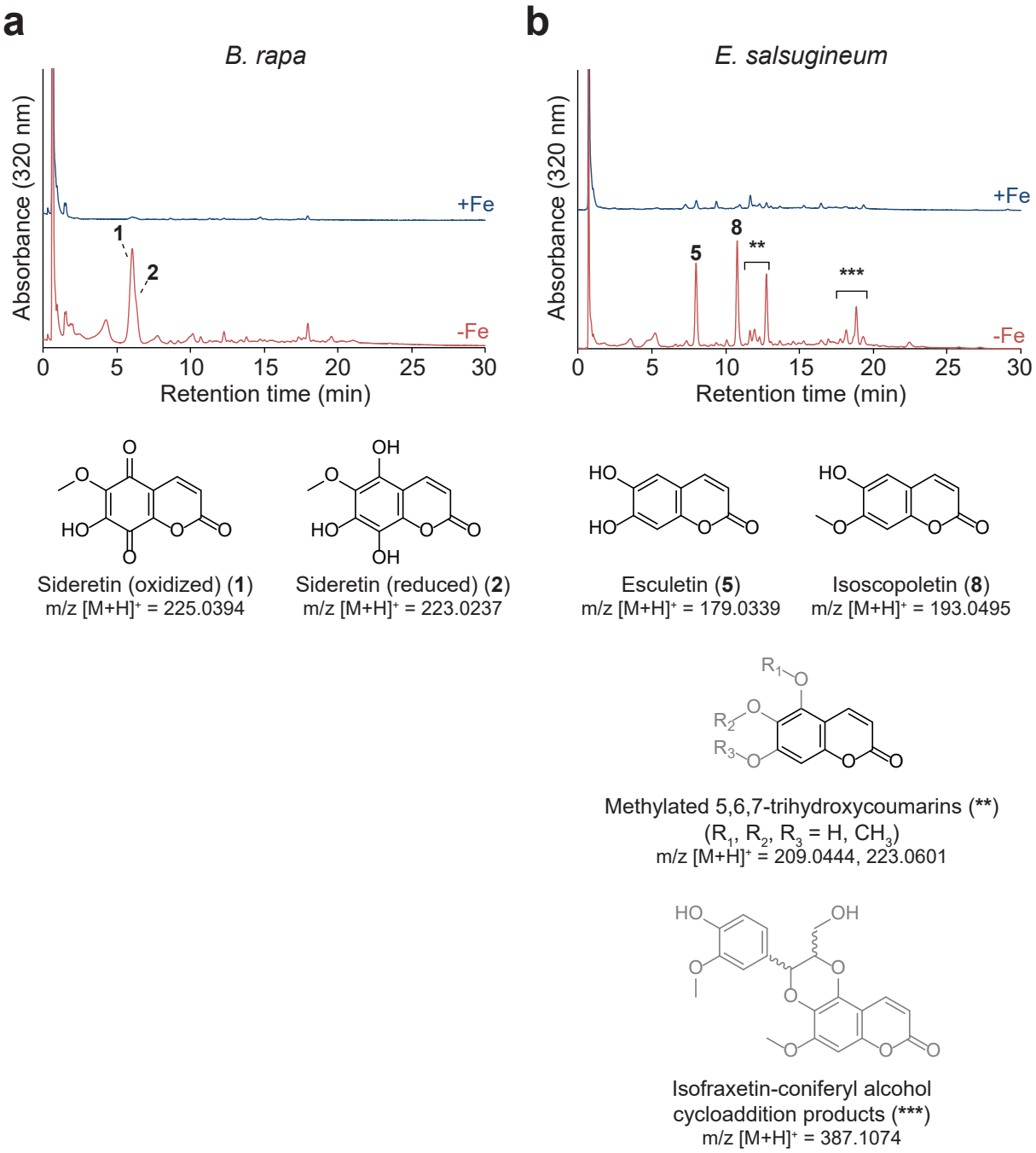

Supplementary Figure 18 (Legend on following page)

Supplementary Figure 18 | Iron deficiency-induced root exudation of oxidized coumarins by other species in the Brassicaceae family. (a, b) Comparison of UV-Vis absorbance traces for spent medium extracts of hydroponically grown *B. rapa* (a) and *E. salsugineum* (b) grown under Fe-sufficient (+Fe) or Fe-deficient (-Fe) conditions; data are representative of three biological replicates. Structures of compounds shown in black were confirmed by comparison with authentic standards, while those in gray were inferred from m/z values and chromatographic properties. In particular, for *E. salsugineum* (b), the peak cluster labeled with "**" includes various methylated isomers of a triply hydroxylated coumarin, but none of these correspond exactly to fraxetin or its methylated derivatives; likewise, cluster "***" consists of peaks with masses matching those of fraxetin-coniferyl alcohol cycloaddition products (see Supplementary Fig. 6), but distinct by chromatography and MS/MS analysis. In conjunction with the high amount of isoscopoletin observed in these exudates, it is most likely that these peaks correspond to isofraxetin (5,6-dihydroxy-7-methoxycoumarin) and derivatives, for which standards were not easily obtainable.

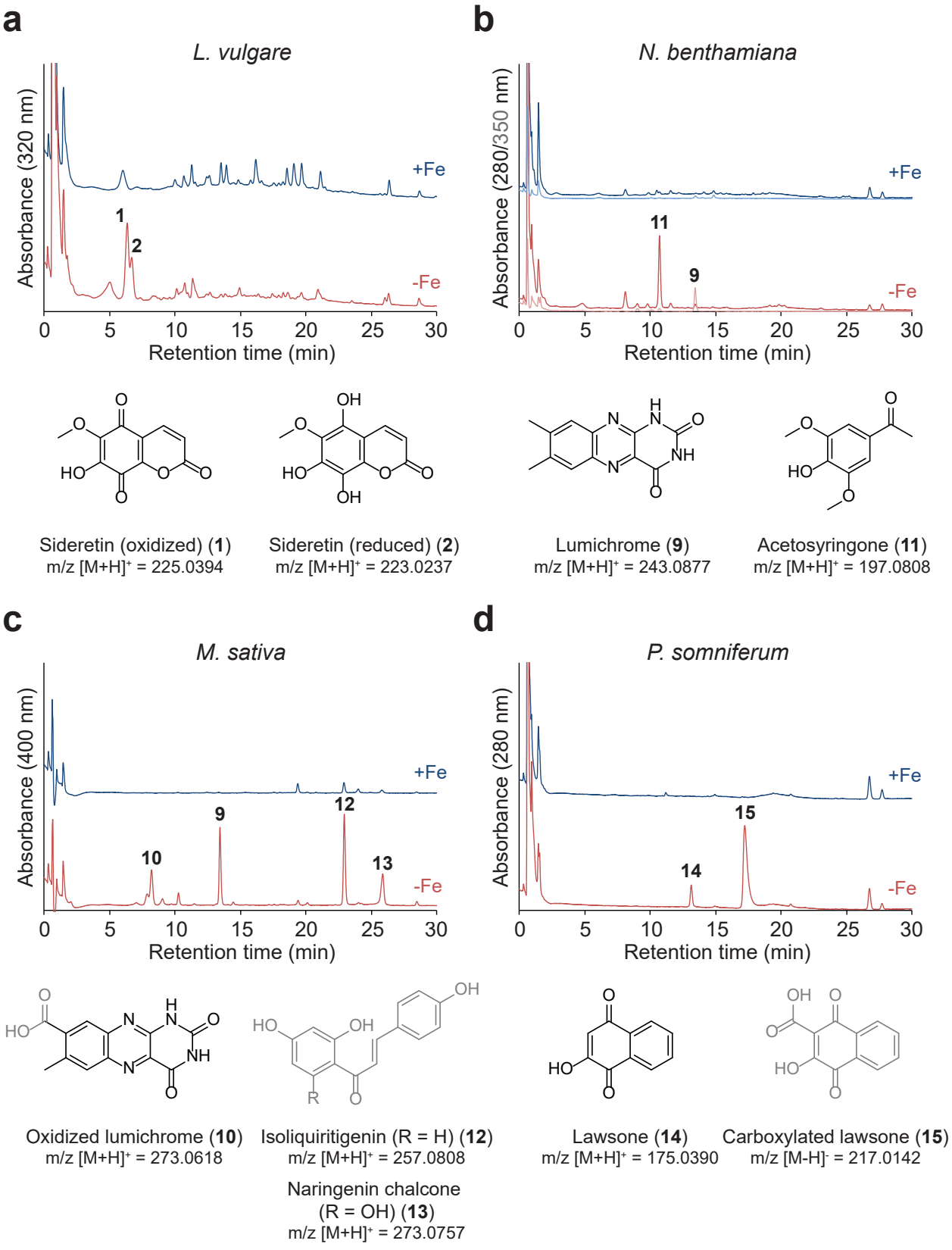

Supplementary Figure 19 (Legend on following page)

Supplementary Figure 19 | Iron deficiency-induced root exudation of structurally diverse compounds by various eudicot species. (a-d) Comparison of UV-Vis absorbance traces for spent medium extracts of hydroponically grown *L. vulgare* (a), *N. benthamiana* (b), *M. sativa* (c), and *P. somniferum* (d) grown under Fe-sufficient (+Fe) or Fe-deficient (-Fe) conditions; data are representative of three biological replicates. As in Supplementary Fig. 18, structures shown in black were confirmed by comparison with authentic standards, while those in gray were inferred from m/z values and chromatographic properties. For *M. sativa* (c), assignment of the two late-eluting compounds **12** and **13** as isoliquiritigenin and naringenin chalcone, respectively, was additionally motivated by previous reports of their occurrence in this species, as well as distinctive UV-Vis absorbance profiles.